Repairable Seismic Moment Frames with Bolted WT Connections: Part I

PATRICK S. MCMANUS and JAY A. PUCKETT

ABSTRACT

A moment frame lateral load-resisting system was developed in which inelastic deformations due to seismic loading were intended to be isolated to easily replaceable WT components. Fully bolted connections were utilized to facilitate simple component installation and replacement. In Part I of this series, WT components for the moment frame system were modeled using finite element analysis. Full-scale component testing was performed to verify analytical results. Parameters taken from modeling and testing results were used to develop design provisions. In Part II of this series, an example building was designed using the provisions developed and analyzed under simulated earthquake accelerations to develop appropriate seismic performance factors. WT components designed using recommended geometric parameters resulted in desirable behavior. Recommended design equations correlated well to experimental test results. Experimental results suggested WT components designed using the recommended provisions exhibit adequate low-cycle fatigue performance and deflection capacity to be used with wide flange beams up to a nominal depth of 30 in. (762 mm). Nonlinear time-history analysis suggests seismic performance factors currently published for steel special moment frame systems are appropriate for the proposed WT moment frame system.

Keywords: partially restrained WT connection, seismic moment connection, finite element analysis, nonlinear analysis, performance-based seismic design.

According to the Hazards U.S. Multi-Hazard (HAZUS-MH) analysis performed by the Federal Emergency Management Agency, the costs associated with a catastrophic seismic event are significant (FEMA, 2008). It can be argued, however, that the many indirect, long-term costs, which are difficult to measure and are admittedly neglected by FEMA, may have an even greater impact. As evidenced by the aftermath of Hurricane Katrina, a catastrophic event can produce societal effects on an area that necessitate years, or even decades, of recovery. By mitigating the initial impact of a significant seismic event and, more importantly, by reducing the direct costs and duration of repair and recovery for the building inventory in a given area, long-term costs can be dramatically reduced.

Seismic load resisting systems for structural steel buildings have undergone considerable evolution over the past 15 years. The major theory driving current design approaches is to provide systems that remain stable under relatively large story drifts while simultaneously experiencing controlled inelastic deformations to dissipate energy (FEMA, 2003). As can be seen by various systems described in the 2005 AISC *Seismic Provisions for Structural Steel Buildings* (AISC, 2005a), this is primarily accomplished by proportioning elements such that specific major components experience inelastic deformations. In addition to components that are not intended to resist lateral loads, components that connect major lateral-load-resisting elements are anticipated to remain substantially elastic and undergo minimal damage. While the idea of isolating large deformations to anticipated components and locations has considerable merit, the current design methods that apply this concept have some inefficiencies and shortcomings; specifically, considerable field welding is often required and inelastic deformations are intended to occur in primary beams or braces.

Primary structural components such as beams and columns are extremely expensive by structural standards and are difficult to adequately repair or replace, particularly when equipped with fully welded connections. Typically, these components are, by design, fully integrated with the overall structural scheme and, in most cases, are relied upon to carry gravity loads in addition to lateral loads. Therefore, repair of such components after significant damage is often not prudent or realistic, leaving replacement as the only viable option. The resulting expense to the owner or insurer from a significant seismic event could be unmanageable, particularly when considering the additional indirect costs associated with having a building out of service for a considerable period of time. For essential facilities where demolition is not an option, difficult in-service repairs also compound the cost.

New innovations in seismic load resisting systems have recognized that the approach of isolating inelastic

Patrick S. McManus, P.E., S.E., Ph.D., Structural Technical Director, Martin/Martin Inc., Lakewood, CO (corresponding author). E-mail: pmcmanus@martinmartin.com

Jay A. Puckett, P.E., Ph.D., V.O. Smith Professor, Department of Civil and Architectural Engineering, University of Wyoming, Laramie, WY. E-mail: puckett@uwyo.edu

deformations to primary, permanently attached components may not be an appropriate solution (Malley, 2000). Instead, by isolating inelastic deformations to easily accessible, bolted components that can be relatively inexpensively removed and replaced, a serviceable seismic load resisting system can be achieved. Herein, a *serviceable*—or easily repairable—*system* is defined as one in which inelastic deformation has been accommodated in such a way that the damaged elements can be reasonably removed and replaced with similar elements after a significant seismic event. Other elements that cannot be reasonably removed and replaced remain substantially elastic and can remain in service.

Serviceable seismic-load-resisting systems, which lend themselves to a performance-based design approach, offer many advantages. Components that are relatively easy to replace are characteristically easy to install initially. Therefore, the field labor associated with the initial installation of a serviceable system may be reduced over the current labor-intensive installation processes that involve considerable field welding.

To adequately address a wide spectrum of building program needs, proposed serviceable connections and components have been developed for moment frame and braced frame systems. Only the moment frame system, referred to as ductile WT moment frames (DWTMF) is addressed here. For maximum economy, in addition to the aforementioned potential reduction in field labor, the proposed systems utilize readily available or easily fabricated components designed to carry minimum force levels as required by the applicable building code.

The results from the evaluation of the DWTMF system indicate that only 18 standard milled WT sections may suitably achieve the required deformation for special moment frame (SMF) systems. The modeled performance of these sections, however, is promising. The sections can also be used with a variety of beam depths, making the system relatively versatile. Reasonable provisions for the selection of the WT section and associated bolt configurations, as well as for the design of all components within the WT connection, are developed. The design of an example building using the recommended provisions is presented and appears viable. Appropriate seismic design coefficients and factors are evaluated as part of a design example. Design aids using the recommended provisions are also presented.

BACKGROUND

Seismic Design Overview

The performance criteria for seismic design currently adopted by reference in the 2006 International Building Code (IBC) are based on preserving life safety by avoiding major structural failure or collapse (FEMA, 2003). In achieving these criteria, structures are anticipated to experience inelastic deformations within the primary structural system during significant seismic events (ASCE, 2005). A return period of 2,475 years (2% probability of exceedance in 50 years) is used to develop the magnitude of the accelerations associated with the maximum considered earthquake (MCE) in most regions. Based on the judgment of the Building Seismic Safety Council (BSSC), a determination was made that structures will exhibit adequate resistance to collapse if the MCE accelerations are reduced by a factor of 1.5 (FEMA, 2003), which would then be the basis for the elastic design of a structure subjected to seismic loading. Designing a structure to remain elastic during a seismic event has been determined to be cost prohibitive for most types of structures; consequently, some degree of inelastic behavior within the primary structural system is assumed for typical building design (ASCE, 2005). Using conventional inelastic design, the return period for a seismic event anticipated to result in inelastic deformations within a structure can range from less than 25 years to 500 years, depending on the site and level of ductility assumed (Malhotra, 2005). Therefore, it is probable that a structure will experience inelastic deformations during the course of its service life in high seismic regions.

Serviceable Moment Frame Seismic Systems

While research has been conducted on several types of bolted moment connections, bolted-bolted WT stub moment connections can be constructed economically and have shown great potential to isolate inelastic deformations to the connecting elements. WT stub moment connections (see Figure 1) have been used in steel construction in the United States for nearly 100 years. Depending on certain parameters (e.g., size of the WT section used, bolt gage on the WT flange, bolt configuration), these connections can meet the stiffness requirements for fully restrained connections or can perform as relatively flexible partially restrained connections. The behavior of the bolted assembly is complicated with respect to both strength and stiffness. Deformation and strength characteristics of the WT flange, WT stem, tension in the bolts at the WT flange and bolts at the WT stem can all influence performance. The effects of prying action on the WT flange, friction and potential slip between the WT stem and beam flange, and deformation at the bolt holes in the WT stem and beam flange further complicate the behavior of the assembly (FEMA, 2000).

While past research has primarily addressed the strength of WT stub connections, Swanson and Leon (2000, 2001) focused on exploring potential failure modes and stiffness characteristics. The research revealed several component or main member brittle rupture failure modes, as well as four ductile yield mechanisms. The yield mechanisms were shear yielding of the column, local flexure of the WT flange, tension yielding of the WT stem and flexural yielding of the beam.

WT stub connections can be designed as either full strength or partial strength. Full strength implies the connections are capable of developing the available strength of the beam, whereas the capacity of partial strength connections is less than the available plastic strength. The available flexural strength of the WT flange can vary greatly with variations in WT flange thickness and the bolt gage on the WT flange. WT flange strength is typically increased by minimizing the bolt gage and/or increasing the flange thickness, adjustments that also result in increased stiffness. Swanson and Leon (2000, 2001) concluded that under certain parameters, significant plastic deformation can occur within the WT connecting element, with the best performance achieved through flexural deformations of the WT flange coupled with tensile deformation of the WT stem (FEMA, 2000). Configurations that allowed for large deformations within the WT exhibited significantly more ductility and joint rotational capacity than stiffer configurations.

WT stub configurations that invoke substantial bending in the WT flange provide increased connection ductility, but they also have decreased stiffness. Therefore, isolation of the inelastic deformations to WT components results in partially restrained (PR) connections. Use of these connections necessitates a more robust analysis that takes into consideration the load-deformation behavior of the connection in addition to that of the primary members (AISC, 2005c). Accuracy of the global model is thus dependent upon the accuracy of the representation of the connection stiffness. A monotonic stiffness model for WT stub connections that takes into consideration the nonlinear behavior of many components within the connection (i.e., tension bolt stiffness, plastic or partially plastic WT flange hinges, slip and bearing at shear bolts) was developed by Swanson and Leon (2001). This complex model has many parameters and lends itself to computer-based solutions. The model may be greatly simplified, however, by limiting the force levels in many of the component mechanisms such that a relatively linear behavior is maintained while inelastic flexural deformations are induced in the WT flange. This approach to connection stiffness is discussed in further detail later.

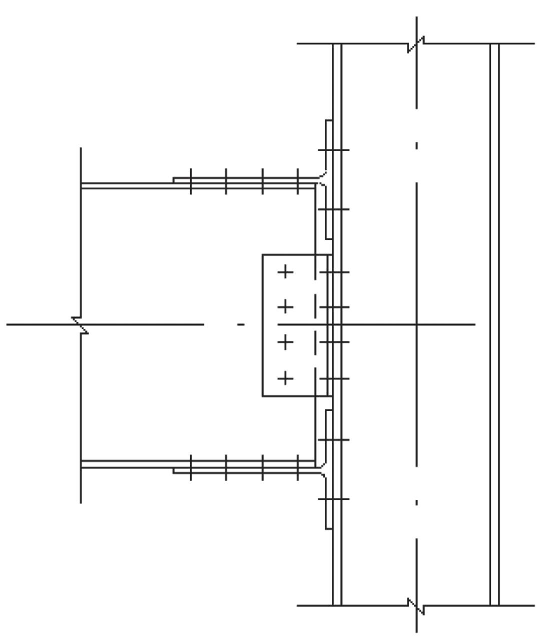

Fig. 1. WT moment connection.

The 13th edition AISC *Steel Construction Manual* (AISC, 2005c) presents a prescriptive approach for determining the available plastic flexural strength of a WT flange and the required available strength of the tension bolts due to additional forces resulting from prying action. A diagram of the geometry and forces considered in this approach is shown in Figure 2. Differing from previous editions of the AISC *Specification*, the 2005 AISC *Specification for Structural Steel Buildings* (AISC, 2005b) determines flange strength in terms of the rupture strength of the WT material, which more accurately represents the actual strength of the flange. However, plastic yield strength of a WT flange can be determined using similar equations as presented in draft design provisions prepared for the AISC Connection Prequalification Review Panel (AISC, 2007). Using the Load and Resistance Factor Design (LRFD) approach, the design resistance per tension bolt is calculated as

$$\phi T_n = \frac{\phi p F_{yt}\left(1+\delta\right) t_{ft}^2}{4b'} \tag{1}$$

where

p = tributary length per pair of bolts, equal to the sum of half the distances to the adjacent bolts or

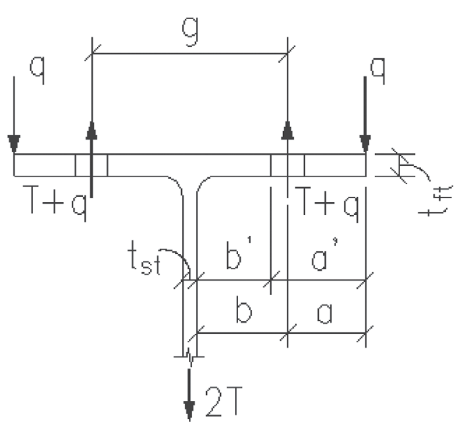

Fig. 2. WT geometry and prying forces.

member edge, but not more than the gage between the pair of bolts, g, in. (mm)

F_{yt} = specified minimum yield stress of the WT material, ksi (MPa)

δ = $1-\dfrac{d'}{p}$ = ratio of the net area at the bolt line to the gross area at the face of the WT stem

d' = width of the hole along the length of the WT (hole size plus $\frac{1}{16}$ in. (1.6 mm) for round holes), in. (mm)

t_{ft} = thickness of the WT flange, in. (mm)

b' = $b-\dfrac{d_b}{2}$, in. (mm)

d_b = bolt diameter, in. (mm)

The approach within the 2005 AISC S*eismic Provisions* is for connections and/or components to be designed with sufficient strength to develop the expected available yield strength of a particular member mechanism. The expected strength of the yielding member is calculated by multiplying the available nominal strength of the member mechanism by the ratio of the expected member yield stress to the specified minimum yield stress. An additional multiplier, described herein by the variable ω, is implemented in some systems to account for strain hardening and/or other sources of overstrength. Therefore, to ensure development of the plastic flexural WT flange-yielding mechanism, the probable design load for all other limit states of a WT stub moment connection per bolt is calculated as

$$P_{pr} = \frac{\omega p R_y F_{yt}\left(1+\delta\right) t_{ft}^{\,2}}{3b'} \tag{2}$$

where R_y is the ratio of the expected yield stress to the specified minimum yield stress of the WT material as defined in the 2005 AISC *Seismic Provision*s. Note that the coefficient in the denominator of Equation 2 was adjusted to a value of 3 rather than the value of 4 used in Equation 1. This was done to express the probable strength, assuming ASTM A992 steel, in terms of yield strength rather than rupture strength, while still achieving a similar prediction.

Commonly used metal deck support details and relatively thin rigid-insulation blockouts in concrete slabs can be utilized to accommodate deformations within the WT in addition to providing access to relatively simple replacement of the WT at the top flange of the beam. Conceptual deck support and slab block-out details are presented in McManus (2010). The presence of a concrete slab could significantly affect the behavior of the connections proposed herein. Concrete slab joint details that allow separation at moment columns while adequately transferring diaphragm and gravity shear forces may be necessary to achieve desirable connection behavior. Slab considerations such as these are not addressed further herein, but they are recommended for study in future work.

DUCTILE WT MOMENT FRAME ANALYTICAL MODELING

Ductile WT moment connections are intended to invoke inelastic deformations in the WT flange while the connected beam and column remain elastic. Thus, the replaceable element experiences the most significant damage. The initial hypothesis supposed that once accurate load distributions of forces in the WT were known, relatively simple proportioning of the gage of the bolts on the WT flange would ensure initiation of flange yielding. The intent was also to verify whether the prying behavior and strength predictions presented in the 13th edition AISC *Manual*, as modified in Equation 2, were adequate to predict the expected yield strength of the WT under large deformations. Also of critical importance are accurate stiffness parameters for the design of the WT. The research was intended to develop load-deflection parameters for the design of moment frames using partially restrained connections.

Nonlinear inelastic time-history analyses were executed using enforced displacements. By conservatively assuming all frame rotation in a ductile WT moment connection is due to the deformation of the WT at the tension flange of a beam of depth, d, the required deflection of the WT, Δ, corresponding to the interstory drift angles, θ (as specified in Appendix S, Section S6.2 of the 2005 AISC *Seismic Provisions*), can be calculated as $\Delta = d \sin\theta$. This relationship is shown graphically in Figure 3, which depicts Δ as the deflection due only to deformation of the WT flange and

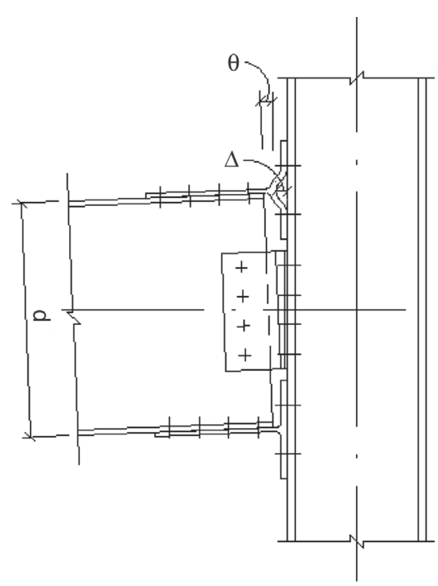

Fig. 3. Assumed connection rotation.

flange bolts. Realistically, deformations from other sources such as the WT stem and bolted connections of the WT stem to the beam flange also contribute to Δ. Using this equation for Δ, the deformation associated with a 44-in. (1120-mm)-deep beam and a 0.04-rad rotation, as required for special moment frame systems within 2005 AISC *Seismic Provisions*, is 1.76 in. (45 mm), which set the target deformation, Δ_{target}, used for all models.

An accurate understanding of the behavior of the WT component under various bolt configurations is a primary concern for proper performance of the ductile WT moment frame system. Therefore, a progressive series of local modeling of various WT specimens was performed in five phases. Finite element analysis of WT stub assemblies performed by Swanson et al. (2002) was used as a basis for developing the finite element models analyzed herein. All WT specimens were 14 in. (356 mm) long. Each WT was modeled with four vertical columns of bolts, two at 5-in. (127-mm) gage and two at 11-in. (279-mm) gage. These parameters provide a reasonable configuration for attachment to large W14 column sections, which are commonly used in seismic moment frames.

Finite element analysis of the WT sections was performed using the FEA program Abaqus (Version 6.8-1). Through the progression of modeling phases, model complexity increased while configurations exhibiting desired behavior were also refined. The first phase of modeling involved 81 configurations consisting substantially of the least-weight and greatest-weight sections in each wide flange size group. Bolt gages of 4, 6 and 11 in. (102, 152 and 279 mm, respectively) were modeled sparingly to encapsulate a large range in proportionality of bolt gage to WT flange thickness. Several modeling simplifications were implemented in the first phase. For example, uniform 2-in. (51-mm)-diameter bolt heads/nuts were used for all models consistent with 1-in. (25-mm)-diameter ASTM A325 or ASTM A490 bolts. Similarly, a uniform radius of the fillet between the WT stem and flange of 0.5 in. (13 mm) was assumed for all sections. Bolt heads/nuts were not included in the model but were simulated with a round surface boundary condition fixed in translation out of the plane of the WT flange. The surface between the WT flange and rigid support plate behind the WT was modeled as frictionless. Furthermore, the simulated bolt head boundary conditions were allowed to translate vertically in the plane of the WT flange to negate the influence of any axial strut action of the WT flange. Friction and strut action were considered in later analyses once the behavior was better understood.

The WT material for the first phase was simulated as elastic perfectly plastic. The yield stress used within the model was 60.5 ksi (417 MPa). This yield stress was the result of assuming ASTM A572 Grade 50 or ASTM A992 steel with a 50-ksi (345-MPa) minimum yield strength multiplied by a factor of 1.1, corresponding to the expected

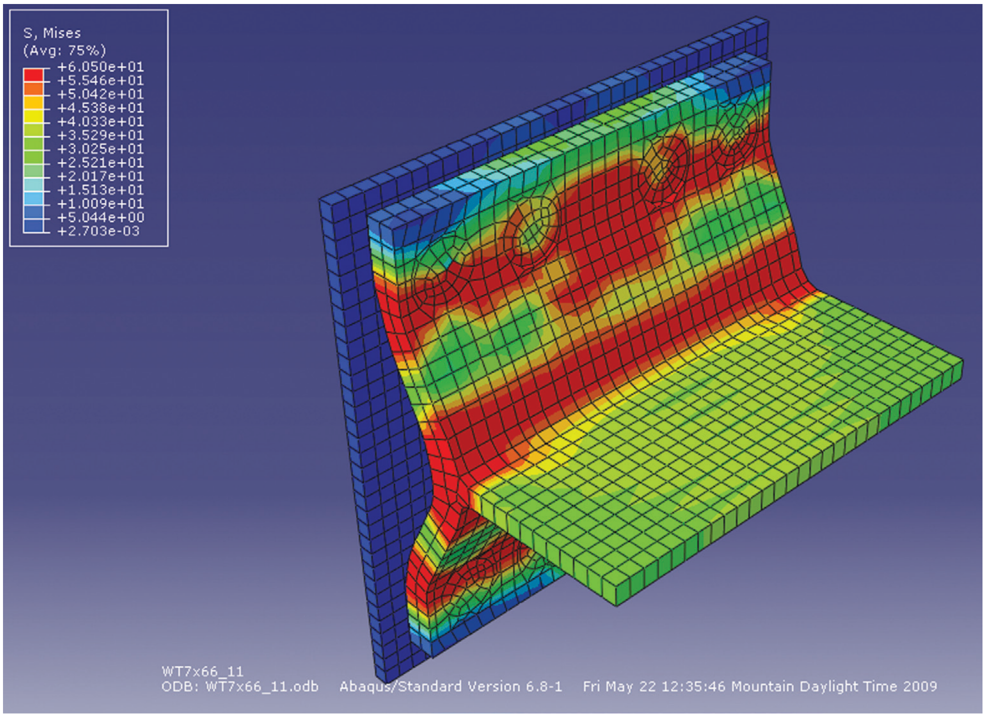

Fig. 4. Stress plot and deformed shape for phase 1 model.

Table 1. WT Sections for Finite Element Analysis (Phase 5)					
Section	Gage on WT, in. (mm)	Bolt Diameter, in. (mm)	Section	Bolt Diameter, in. (mm)	Gage on WT, in. (mm)
WT20×99.5	12 (305)	1.25 (32)	WT7×72.5	11.75 (298)	1.375 (35)
WT18×115.5	12.5 (318)	1.375 (35)	WT7×66	11.25 (286)	1.25 (32)
WT18×67.5	9 (229)	1.125 (29)	WT7×60	10.75 (273)	1.125 (29)
WT16.5×110.5	12.25 (311)	1.375 (35)	WT7×54.5	10.5 (267)	1.125 (29)
WT16.5×100.5	12 (305)	1.375 (35)	WT7×49.5	10 (254)	1 (25)
WT15×86.5	11.5 (292)	1.375 (35)	WT7×45	9.75 (248)	1 (25)
WT13.5×73	10.75 (273)	1.25 (32)	WT6×39.5	9.5 (241)	1 (25)
WT12×52	9.25 (235)	1 (25)	WT6×36	9 (229)	1 (25)
WT7×79.5	12 (305)	1.375 (35)	WT6×32.5	8.5 (216)	0.875 (22)

yield overstrength factor, R_y, defined in Equation 2. The aforementioned overstrength factor, ω, was taken as 1.1 to account for strain hardening consistent with other seismic systems outlined in the 2005 AISC S*eismic Provisions*. A stress at first yield, which included the strain-hardening factor, was assumed to simplify the model and, hopefully, to result in a conservative yield force that might offset omitting the aforementioned friction and axial. Because of the unpredictability and assumed minimal influence of residual stresses on the expected available strength of the WT connections, residual stresses were not considered within the models. An example of a deformed model from the first phase is shown in Figure 4.

The second, third and fourth phases of modeling involved progressive increases in complexity, refinement of geometric parameters resulting in a configuration exhibiting desirable behavior, and development of equations for a bi-linear model to predict load-deformation behavior. The fifth phase involved all 18 configurations that met the geometric provisions and strength requirements resulting from the prior phases. Two geometric limits were developed as a result of the experimental testing. The geometric parameter required to ensure flange yielding occurs prior to stem yielding is

$$\lambda_{WT} = \frac{b^*}{t_{ft}^2} t_{st} \geq 1.14 \tag{3}$$

where

$$b^* = \frac{g}{2} - k_1 - d_b \text{, in. (mm)} \tag{4}$$

g = bolt gage on the WT flange, in. (mm)

k_1 = distance from the centerline of the WT cross-section to the toe of the fillet on the WT flange, in. (mm)

d_b = diameter of the bolt, which is approximately the radius of a standard washer, in. (mm)

t_{st} = thickness of the WT stem, in. (mm)

The geometric parameter required to ensure stem yielding does not initiate, or is minimized, at large deformations is

$$b^* \geq 1.75 \text{ in. (44 mm)} \tag{5}$$

The sections analyzed in the fifth phase of modeling are presented in Table 1. Details are outlined in McManus (2010).

Modeling was consistent with the work performed by Swanson et al. (2002). Shaft components were modeled to represent bolts. An enforced translation on the bolt shafts was imposed in the initial time step to simulate bolt pretension. Oversized holes were modeled in the WT flange to facilitate erection fit-up by accounting for potential overrun and underrun in wide flange beams due to standard mill processes. Oversized holes were also used to allow the WT flange to translate vertically along the column flange without engaging bearing on the bolts. This was done in an attempt to reduce axial restraint of the flange and to postpone the formation of axial strut behavior, as well as to postpone placing significant shear in the bolts. Consistent with the work performed by Swanson et al., stress-strain points were used to simulate strain hardening in the material deformation curves for the WT component, support plate and bolts. Consistent with 2005 AISC *Specification* provisions for a Class A faying surface, a friction coefficient of 0.35 was used between the back of the bolt head/nut elements and the front of the WT flange. This friction coefficient was also used between the back of the WT flange and the front of the support plate. An example of a deformed model from the fifth phase of modeling is shown in Figure 5.

By the fifth phase of modeling, the overstrength factor was adjusted to the following empirical value to account for effects of material and geometric (axial strut action) overstrength:

$$\omega = 1.5\sqrt[3]{\frac{3.5}{b^{*} t_{ft}}} \tag{6}$$

The strength predictions calculated using Equation 2 with the overstrength factor of Equation 6 produced results with an average error of 8.5% and a maximum error of 16.7% when compared to the analytical results, which were relatively consistent with the fourth phase of modeling. Because a relatively simple equation was used to represent complex behavior, these errors were deemed reasonable. Additional equations used to define the bi-linear stiffness model mentioned previously are summarized later in this paper.

DUCTILE WT MOMENT CONNECTION EXPERIMENTAL TESTING

Test Equipment, Arrangement and Procedure

Various WT specimens were tested in two phases. The first phase involved testing a variety of sections and parameters—some falling outside the geometric parameters developed as a result of the analytical modeling, and others falling within the recommended parameters that were expected to induce flange yielding with little or no stem yielding. The intent of this phase of testing was to validate the recommended geometric parameters. The second phase involved sections with configurations matching those from the fifth phase of analytical modeling. The intent of testing these sections was to verify the expected strength and stiffness predictions presented later and to verify acceptable ductility of the assemblies by meeting the cyclic loading criteria specified in Appendix S of the 2005 AISC *Seismic Provisions*. Two WT6×32.5 sections with the same bolt configuration were tested in phase 2 in an effort to demonstrate repeatable results.

To perform these various tests, a test frame with an actuator rated to produce a 600-kip (2850-kN) compressive force and 450-kip (2140-kN) tensile force was constructed as shown in Figure 6. Oversized holes as defined by the 2005 AISC *Specification* were used in the WT flanges and were consistent with the analytical models.

The actuator was used to produce deformation-controlled loading of the WT specimens. A simple, monotonically increasing load was applied to the phase 1 test specimens until a rupture limit state or the target deformation of 1.775 in. (45 mm) was achieved for comparison to the analytical modeling results. Phase 2 specimens were tested using a loading sequence consistent with Appendix S in the 2005 AISC *Seismic Provisions*. This loading sequence is presented

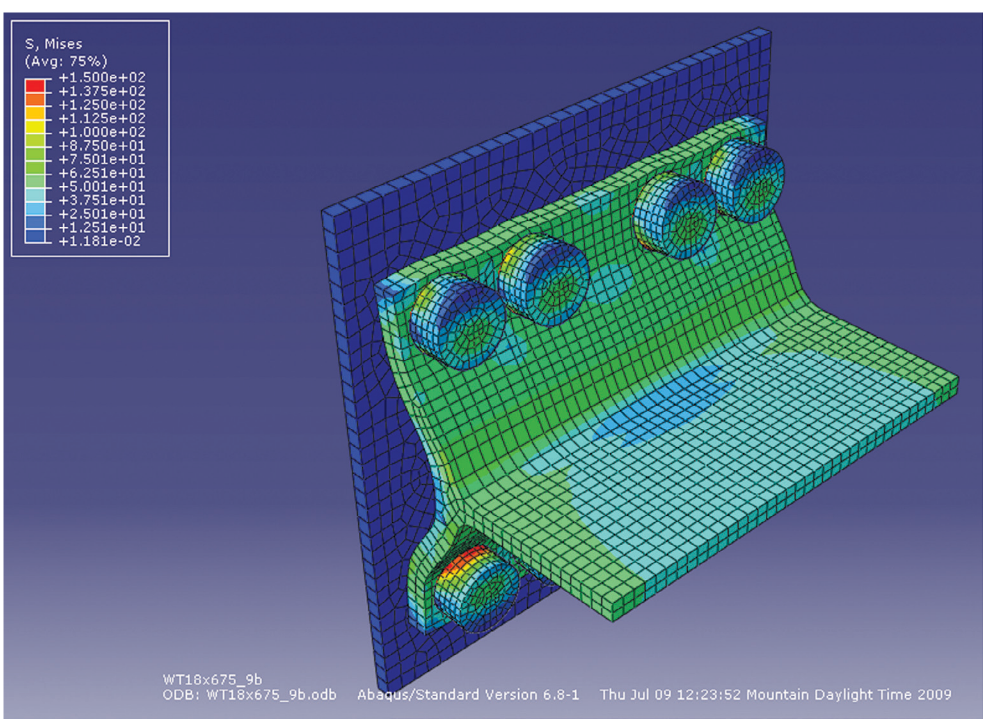

Fig. 5. Stress plot and deformed shape for phase 5 model.

graphically in Figure 7. An intermediate load rate of approximately 0.2 in. (5 mm) per second was used.

Pressure sensors were present at the top and bottom of the actuator (each side of the piston). Readings from these sensors were used to calculate the force applied by the actuator. Relative deflection between the actuator casing and the end of the actuator shaft was measured using a linear potentiometer. Because this instrument was the least susceptible to damage during testing and most representative of the overall deformation of the WT assembly, data from this sensor were used to control the actuator. The disadvantage of using this sensor was that any deformation in the test frame would also be included in the measurements. As shown in Figure 8, separation of the WT flange from the support was measured directly using optical position sensors. These data were intended to be used to assess the portion of total deformation that occurs in the WT flange and, coupled with the overall deformation data, to determine that portion of the total deformation associated with the WT stem and test frame.

Strain data were taken at the anticipated locations of the plastic hinges on the WT flange and at the WT stem just past the toe of the fillet. For phase 2 testing, strain data were also taken between the anticipated locations of the plastic hinges on the WT flange as shown in Figure 8.

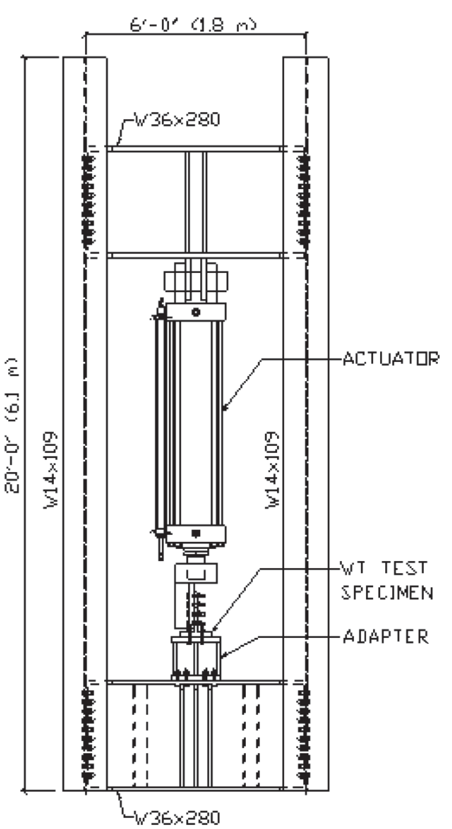

Fig. 6. WT test frame diagram.

Experimental Testing Results

The linear approximations developed in the analytical modeling phase incorporated the expected material yield factor, R_y, in consideration of both yield strength, P_y, and probable strength at the maximum considered deformation, P_{pr}, which were used to approximate the inelastic stiffness. In evaluating the experimental test data, it was recognized that using the expected yield factor likely overpredicted the inelastic portion of the curve, which would be unconservative for collapse analysis of a building frame. Consequently, it was determined the bi-linear curve should be based on the minimum specified material yield strength, F_y, to approximate stiffness for modeling purposes and that the expected yield factor, R_y, should only be used to determine a maximum probable strength for the design of connection limit states and primary members. To produce a direct comparison, the experimental test results were compared to bi-linear curves and maximum strength equations based on the minimum yield strength with no expected yield factor.

Additionally, the actual yield strength from coupon tests was considered in developing the bi-linear curves. Comparisons to the experimental data using the material yield strength from the coupon tests indicated the bi-linear curves overestimated the yield load, and, correspondingly, overestimated the load at the target deformation. In an effort to produce a conservative probable strength throughout the analytical modeling, the width of the WT flange tributary to each bolt, p, was taken as the maximum spacing of 5 in. (127 mm) between any two bolts. Based on comparisons to the experimental results, it was determined that adjusting

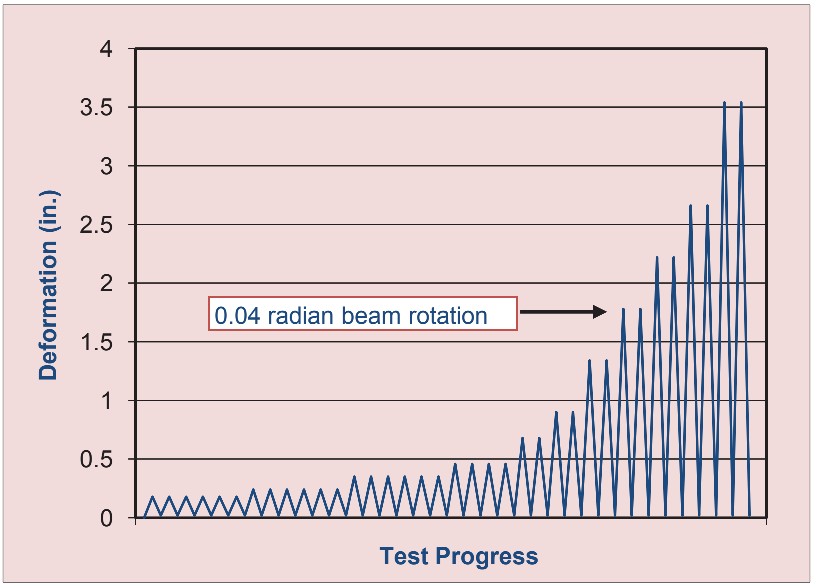

Fig. 7. Load function for testing phase 2.

the tributary width to 4.5 in. (114 mm) improved the correlations and was more appropriate. The bi-linear curves and comparisons to experimental data presented hereafter are based on the use of a tributary width $p = 4.5$ in (114 mm).

The stiffness associated with the elastic portion of the experimental curves was determined in accordance with the recommendations of the FEMA P695 report, "Quantification of Building Seismic Performance Factors" (FEMA, 2009). The stiffness is determined by striking a line from the origin of the load deformation curve through the experimental value corresponding to 40% of the yield strength, which for this research was taken as the theoretical yield strength, P_y. Correlations over the elastic portions of the curve for all test phases were drawn based on the data from the origin through the values at $0.4P_y$. Because the inelastic data vary significantly among testing phases, particularly when considering the cyclic data from phase 2, comparisons of the data over the inelastic portions of the curve are discussed in the following sections.

Phase 1 Experimental Testing Results

The difference between overall deformation and the deformation at the WT flange was assessed in phase 1 of testing. The WT13.5×73 and WT7×45 sections met the recommended geometric provisions determined from the analytical modeling, while the remaining sections did not meet these geometric criteria. For the WT13.5×73 and WT7×45 sections, deformation at the WT flange was 78 and 80% of the overall deformation, respectively, indicating that the majority of the deformation occurred in the flange and flange bolts, as expected. For the remaining sections, the deformation at the WT flange ranged from 45 to 65%, with an average value of 54% of the overall deformation, indicating considerably more deformation was attributed to sources outside the WT flange assembly.

Because the deformation from all sources outside the WT flange assembly was relatively small for configurations

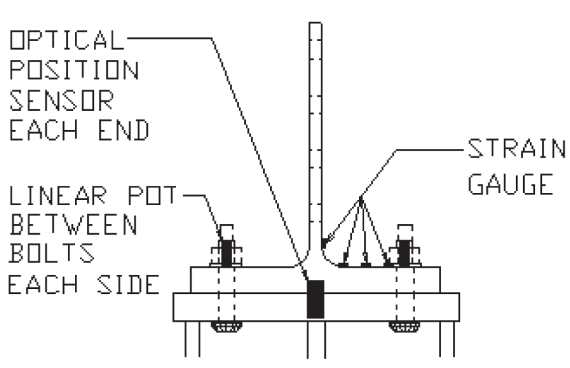

Fig. 8. Phase 2 specimen instrumentation diagram.

meeting the recommended geometric criteria, correlations with the linear approximation equations were made to the overall deformations. Considering overall deformations rather than only deformation in the WT flange results in a more conservative stiffness estimate used to validate the recommended provisions.

Overall correlations for the phase 1 data could be calculated directly because of the monotonic nature of the tests. As summarized in Table 2, the monotonic test data from the two sections that met the recommended geometric criteria correlated well with the linear approximations that were derived from the analytical modeling. The results produced a minimum correlation coefficient of 0.96 over the elastic portion of the curve and an average overall correlation coefficient of 0.97. The final deformed shape of the WT13.5×73 specimen is shown in Figure 9.

Conversely, the average correlation coefficients for the remaining sections that did not meet the recommended geometric provisions were 0.80 and 0.81 for the elastic portions of the curves and overall curves, respectively. More telling are the comparisons of the experimental maximum load to the corresponding theoretical load determined using the linear approximation equations. For the two sections meeting the recommended geometric provisions, the average percent error between the maximum experimental and theoretical loads is 3.0%, while the average percent error for the remaining sections is 71.1%. Example comparisons of the approximated and experimental load-deformation curves for one section meeting and one section not meeting the recommended geometric provisions are shown in Figures 10 and 11, respectively. Material test data from coupon tests were not acquired for the sections not meeting the recommended geometric provisions. Therefore, the bi-linear approximations for these curves were based on an assumed yield strength, $F_y = 55$ ksi (380 MPa), based on the average yield strength from the coupon tests of the other specimens. The result is a recognized potential for error in the bi-linear models for the sections not meeting the recommended geometric provisions, which is likely not more than 10% and has little effect on the conclusions drawn.

The tests of the WT18×75, WT9×79 and WT7×79.5 sections were limited to relatively small deformations because the capacity of the actuator was reached. The limited number of data points for the tests of these three sections could contribute to the poor overall correlations observed. However, overall correlations were consistent with the elastic correlations, suggesting that the poor overall correlations are representative.

The data illustrate that the linear approximation equations are representative of actual behavior for configurations within the recommended geometric provisions. The results, however, also verify the complexity of the behavior of bolted WT sections and indicate that the linear approximation equations do not adequately simulate behavior for configurations that fall outside the recommended geometric provisions.

The sections for the phase 1 testing were designed prior to performing the analytical finite element analyses, and, thus, they were designed before gaining an enhanced understanding of the ultimate strength of the WT configurations. Consequently, the flange bolts were underdesigned for many of the WT strengths expected at large deformations.

The testing was performed with this deficiency recognized, but taken as an opportunity to challenge the recommended bolt design provisions derived from the analytical modeling. The bolt designs for the WT18×75, WT9×79 and WT7×79.5 sections were not challenged because the tests were terminated at relatively small deformations and associated bolt stresses. Conversely, two of the flange bolts in the WT13.5×73 configuration ruptured in a brittle manner at a deformation very near the maximum deformation. The bolts were underdesigned by a factor of approximately 2, suggesting that the bolts would not have failed if properly designed. Therefore, the recommended bolt design provisions appear reasonable.

Further supporting the validity of the proposed recommendations was the dramatic failure of all eight flange bolts during the test of the WT16.5×59 section. This section fell outside the recommended geometric provisions with a ratio of $\lambda_{WT} = 0.88$ in lieu of the recommended minimum value of 1.14, and a value of b^* of 0.875 in. (22 mm) in lieu of the recommended value of 1.75 in. (44 mm), which is approximately equal to Δ_{target}. Additionally, the section was fabricated with standard holes rather than the recommended oversized holes, and the flange bolts were underdesigned by a factor of 2. Bolt failure occurred at an overall deformation of 1.01 in. (26 mm) and deformation at the WT flange of 0.66 in. (17 mm). These values envelop the b^* value of 0.875 in. (22 mm) and support the theory that a value of b^* should be approximately as large at the maximum anticipated deformation, Δ_{target}. While data from the bolts themselves are not available, observation of video footage of the test suggests the bolts were resisting considerable prying forces, bending due to rotation of the flange near the nut and possibly shear because of the use of standard holes.

Perhaps the most important lesson from the test of the

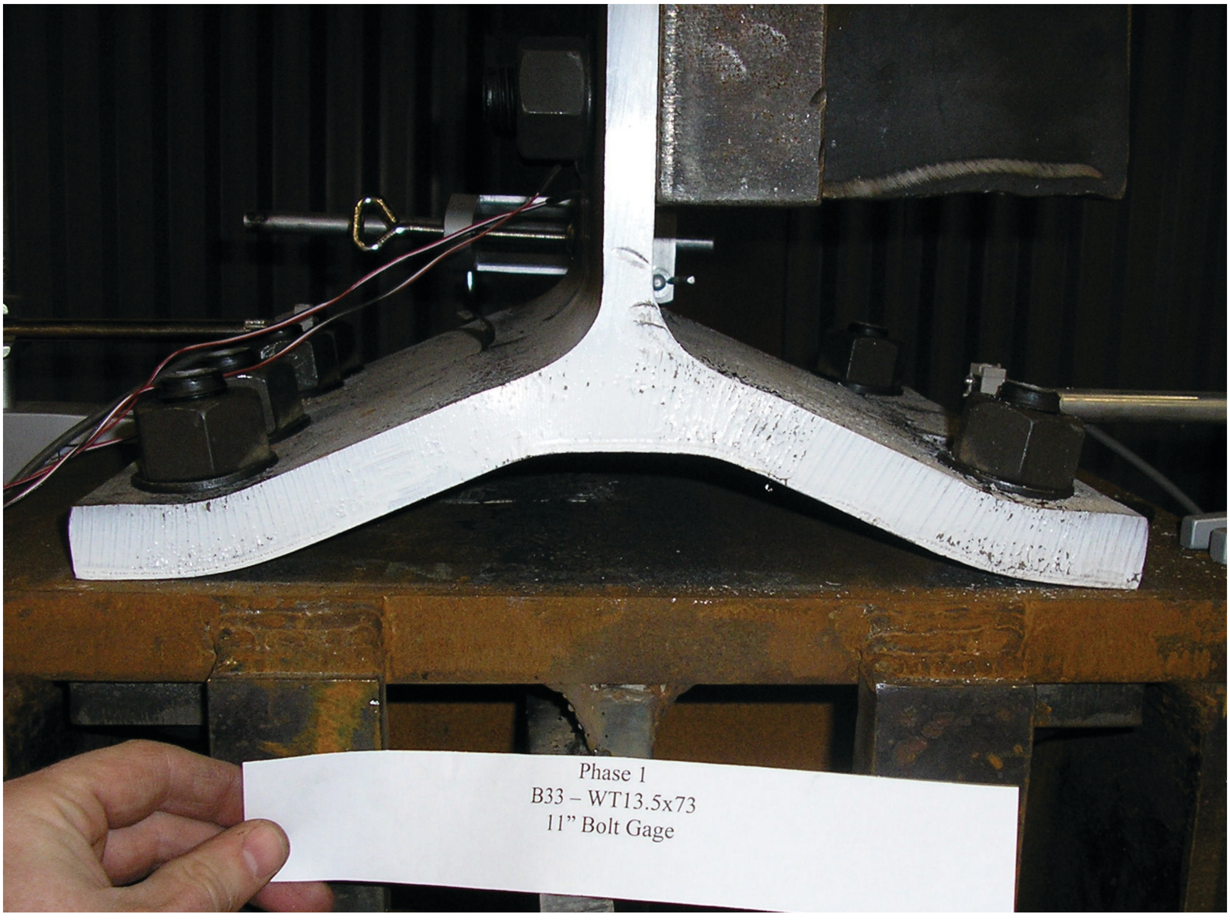

Fig. 9. Deformed phase 1 specimen.

Table 2. Summary of Experimental Testing Results for Phase 1						
Section	Meets Recommended Criteria	Elastic Correlation Coefficient	Overall Correlation Coefficient	Experimental Maximum Load, kips (kN)	Theoretical Corresponding Load, kips (kN)	Error in Load, %
WT13.5×73	Yes	0.97	0.94	352 (1566)	361 (1606)	2.6
WT7×45	Yes	0.96	0.97	214 (952)	221 (983)	3.3
WT18×75	No	0.83	0.87	449 (1998)	752 (3346)	67.5
WT16.5×59	No	0.97	0.95	427 (1900)	578 (2572)	35.4
WT9×79	No	0.70	0.72	449 (1998)	954 (4245)	112.7
WT7×79.5	No	0.68	0.69	376 (1673)	634 (2821)	68.6

WT16.5×59 specimen was recognizing that failure in this manner is entirely unacceptable within an occupied building. At failure, the bolts and nuts projected from the specimen with high velocity sending one nut approximately 20 ft (6 m) into the air, a condition that could impose considerable danger to building occupants. The test reaffirms the importance of adhering to provisions that isolate damage to the WT section, such as the recommended geometric limitations, use of oversized holes and proper bolt design.

In all cases, data from the strain gauges indicated the maximum strains occurred at either the toe of the fillet or near the bolt line within the WT flange. Strains in the stem of the WT7×45 sections approached the theoretical yield strain of 0.0017 in./in. (mm/mm), but did not appear to exceed yield. Stem strains in the WT13.5×73 section exceeded the yield strain near the maximum deformation and associated flange strength. The WT18×75, WT9×79 and WT16.5×59 sections experienced stem envelop strains in excess of theoretical yield near the end of each respective test. This is significant in that these tests were terminated at deformations significantly less than the target deformation, which suggests stem yielding would have continued as axial strut action and the associated increased available strength in the flange were engaged. Therefore, the recommended geometric provisions appear to provide a reasonable threshold to minimize stem strain. The WT7×79.5 did not experience strains in excess of the theoretical yield strain; this is largely attributed to cover plating of the stem to avoid a net section failure and the small overall deformation of 0.34 in. (9 mm), which was reached before the test was terminated.

Phase 2 Experimental Testing Results

The specimens tested in phase 2 performed reasonably well under several criteria. The largest full cycle of deformation at the WT flange and overall deformation (difference between the peak and trough for each instrument) were compared. The proportion of the deformation at the WT flange to the overall deformation was consistent and was slightly improved over phase 1, ranging from 80 to 91% with an average of 85%. Correlations to the linear approximations were again drawn to the overall deformation to pursue a conservative stiffness.

The actual magnitude achieved by the cyclic-loading regimen was of paramount concern to assess the low-cycle fatigue rotational capacity of the proposed connection. Only the WT13.5×73, WT7×66 and WT7×54.5 sections achieved cycles at the target deformation of 1.76 in. (45 mm) before rupture of the flange occurred. Slightly less than one full cycle was reached during testing of the WT7×54.5 section. The remaining sections reached an overall measured deformation of 1.38 in. (35 mm) prior to complete cracking across the WT flange, which corresponds to the set of cycles proceeding the target deformation cycles.

Deformations within the test frame, however, were observed and accounted for to calculate adjusted overall deformations. The frame deformations and adjustment processes are discussed in McManus (2010). The minimum adjusted overall deformation of the specimens tested was 1.08 in. (27 mm), and the average deformation from the specimens that did not achieve the target deformation was 1.18 in. (30 mm). Recognizing the target deformation of 1.76 in. (45 mm) was based on the assumption of a 44-in. (1118-mm)-deep beam section achieving a rotation of 0.04 rad, ratios of the minimum and average calculated deformations to the target deformation result in corresponding beam depths of 27 in. (686 mm) and 30 in. (762 mm), respectively. Based on this assessment, it is recommended the proposed WT configurations are appropriate for beam depths up to approximately 30 in. (762 mm), or W30 wide flange sections, and that this should be the basis for future experimental evaluation of the system.

A summary of the results for the phase 2 testing is presented in Table 3. The elastic portion of the load-deformation curves produced minimum and average correlation coefficients between the experimental data and linear approximation equations of 0.94 and 0.97, respectively. Because a

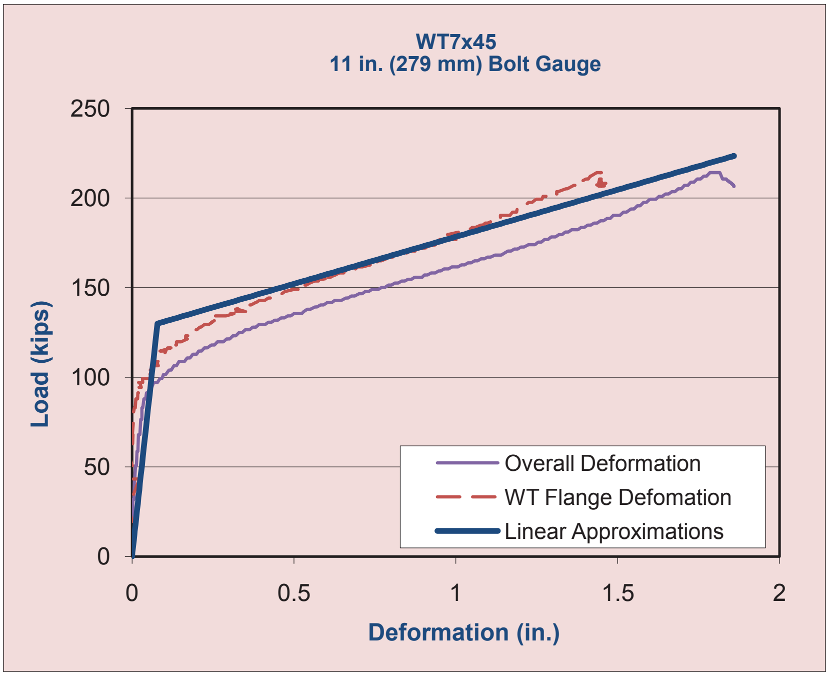

Fig. 10. Example load-deformation plot (section within geometric provisions).

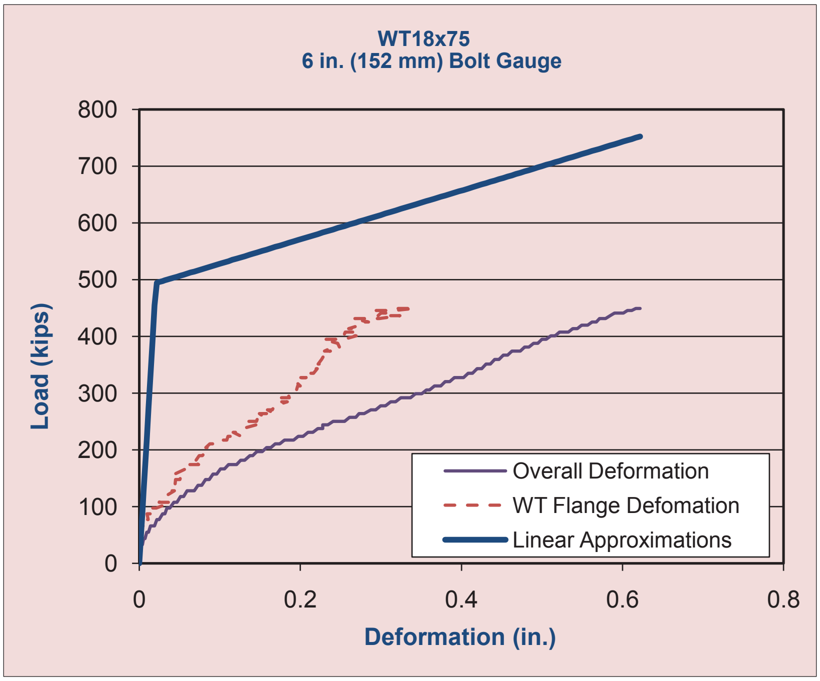

Fig. 11. Example load-deformation plot (section outside of geometric provisions).

Table 3. Summary of Experimental Testing Results for Phase 2					
Section	Elastic Correlation Coefficient	Percent Error in Inelastic Stiffness,%	Experimental Maximum Load, kips (kN)	Theoretical Corresponding Maximum Load, kips (kN)	Error in Maximum Load,%
WT18×67.5	0.98	6.7	321 (1428)	341 (1517)	6.3
WT13.5×73	0.98	34.4	423 (1882)	394 (1753)	6.9
WT7×66	0.98	27.3	390 (1736)	396 (1762)	1.4
WT7×60	0.98	21.0	294 (1308)	304 (1353)	3.4
WT7×54.5	0.99	26.3	332 (1477)	325 (1446)	2.3
WT7×45	0.99	9.5	233 (1037)	241 (1072)	3.3
WT6×39.5	0.96	10.2	237 (1055)	257 (1144)	8.3
WT6×32.5-1	0.94	16.6	209 (930)	205 (912)	1.7
WT6×32.5-2	0.98	15.0	205 (912)	204 (908)	0.8

correlation between the inelastic linear approximation and the cyclic data is difficult to draw, the slope of the inelastic portion of the experimental data was determined using a point near the yield load and a point near the maximum load and was compared to the slope of the inelastic linear approximation equation. The maximum percent error between the two slopes was 34.4%, with an average percent error of 18.6%. The maximum percent error between the maximum experimental and theoretical loads was 8.3%, while the average percent error was 3.8%. These results, coupled with observation of a reasonable envelop of the experimental load-deformation data by the linear approximation curve, suggest the linear approximation equations are appropriate for the range of sections considered. An example load-deformation comparison is presented in Figure 12. Similar plots of other specimens are available in McManus (2010).

In general, strains well in excess of yielding were found in the WT flange at the toe of the fillet, near the bolt line and between these two locations. Strains at the stem remained relatively small and were typically below the theoretical yield strain, with the exception a limited number of peaks for each test that did occur near the maximum deformation. The peaks in stem strain may have been more the result of a buckling mechanism initiating in the compression stroke than of tensile forces or the result of large bending stresses in the stem subsequent to fracture of the flange on one side of web, both of which would explain why the peaks possessed greater magnitude in the phase 2 tests than were observed in phase 1.

Because all sections in phase 2 met the recommended geometric provisions, the strain data suggest the provisions reasonably minimize the strains in the WT stem and isolate damage to the WT flange. The strain gauges had a maximum strain threshold of 5%. Strains in excess of this value produced spikes up to this threshold followed by flat lines at the threshold. Several sections suggested strains at various locations throughout the flange, while in excess of yield, were less than 5% and were significantly lower than the minimum rupture strain of 21% required of ASTM A992 steel. This suggests the flange failures were more the result of low-cycle fatigue than of large strains approaching rupture.

All flange fracture failures occurred at the toe of the fillet in the WT flange as shown in Figure 13. This failure mechanism could be exacerbated by potentially increased bending stresses due to rotation of the beam. Thus, testing of beam-column subassemblies in future work is important to verify the performance of the WT.

While the toe of the fillet is a known location of residual stress and associated weakness in the web of wide flange sections as a result of the mill production and straightening processes, the testing herein clearly exposes a similar weak point at the toe of the fillet in the flange as well. Though the hinge location near the bolt line underwent rotation similar to that of the location at the toe of the fillet, no failures occurred at the bolt line, nor were the initiation of any significant cracks observed. This suggests that larger deformations could be achieved in WT specimens by using a cast and/or tempered WT section rather than rolled. Assuming proper conditions to minimize impurities and grain size, casting a section from scrap ASTM A992 steel may result in reduced residual stresses and associated weakness at the toe of the fillet.

Though the specimens still possessed some load-carrying capacity after facture on one side of the web, tests were terminated shortly after such a fracture occurred to avoid destruction of the instrumentation and the actuator. Therefore, full backbone curves were not developed. In other words, degradation behavior beyond the capping point, or point of maximum load, was not considered (FEMA, 2009). For the purposes of analysis, the sections can be conservatively assumed to lose all load-carrying capacity after a deformation of 1.2 in. (30 mm) is reached, as described previously.

In all phase 2 specimens, significant yielding, and, ultimately, fracture were isolated to the flange of the WT, resulting in a ductile failure mechanism. The limit states of flange bolt rupture, stem bolt rupture, stem net section rupture, stem block shear rupture and stem compression buckling did not govern any of the phase 2 tests, which indicates the recommended strength for the design of these limit states was adequate. The stem did not appear to be susceptible to buckling until rupture of the flange occurred, at which point a significant eccentricity in the stem was created and bending of the web was observed. Significant lateral translation of the WT flange was observed at the flange bolt lines in all tests, which further verifies the need for oversized holes in the WT flange to avoid restraint and additional shear forces in the flange bolts.

RECOMMENDED DESIGN PROVISIONS AND BI-LINEAR MODEL

Recommended design provisions and equations used to develop the bi-linear model based on the results of the analytical modeling and experimental testing are as follows.

Oversized holes as defined within Table J3.3 of the 2005 AISC *Specification* shall be used in the flange of the WT. Standard holes as defined by the 2005 AISC *Specification* shall be used in the flange of the column to which the WT is connected.

The force in the WT at which initial yield in the WT flange occurs, P_y, is taken as

$$P_y = \frac{8pF_{yt}\left(1+\delta\right)t_{ft}^2}{3b'} \tag{7}$$

where p is taken as 4.5 in. (114 mm). The force in the WT, P_ω, at the maximum considered deformation, $\Delta_{max} = 1.76$ in. (45 mm), to be used for the purposes of determining inelastic stiffness shall be taken as

$$P_\omega = \omega P_y \tag{8}$$

where

$$\omega = 1.5\sqrt[3]{\frac{3.5}{b^* t_{ft}}} \tag{8a}$$

The maximum considered deformation corresponds to 0.04 rad of rotation in a nominal 44-in. (1118-mm)-deep beam.

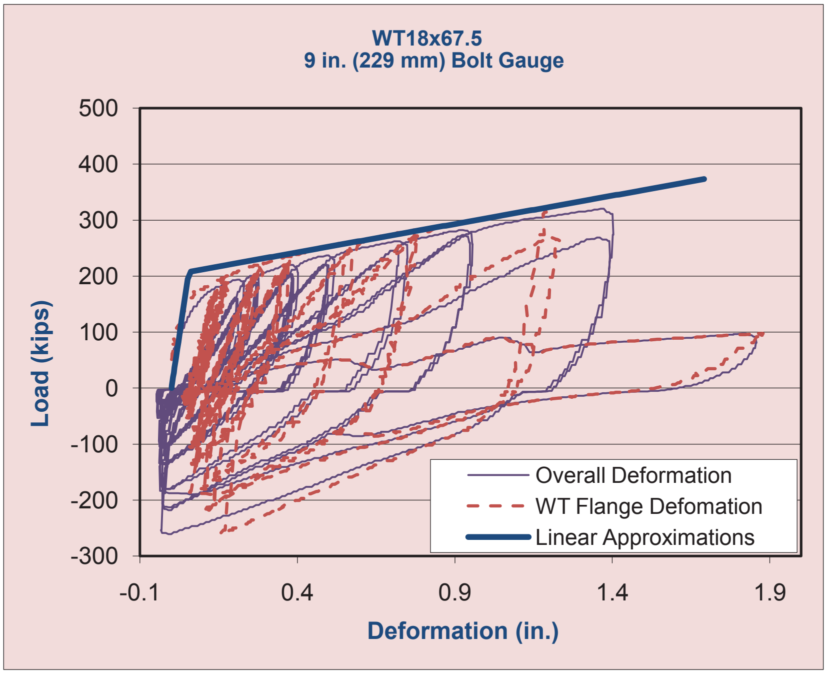

Fig. 12. Example phase 2 load-deformation comparison.

The maximum probable force in a WT used to design (using an LRFD approach) the limit states of stem gross yield, stem net section rupture, stem block shear, stem compression buckling, stem bolt bearing, stem bolt shear, beam flange bolt bearing, beam flange block shear, column flange local bending, column web local yielding, column web crippling and column web panel zone shear may be taken conservatively as

$$P_{pr} = R_y P_{\omega} \tag{9}$$

for all nominal beam depths less than or equal to 30 in. (762 mm). Alternatively, the probable force in the WT as a function of beam depth may be taken as

$$P_{pr} = R_y \left[\left(\frac{\Delta_{target}}{\Delta_{max}} \right) \left(P_{\omega} - P_y \right) + P_y \right] \tag{10}$$

where $\Delta_{target} = d(\sin \theta)$ and θ is the required rotational capacity of the connection, equal to 0.04 rad.

The bolts connecting the WT flange to the column shall be proportioned such that

$$8\left(B - q\right) \geq P_{pr} \tag{11}$$

where B is the available tension per bolt (equal to ϕr_n for LRFD), and q is the prying force calculated as described in the 13th edition AISC Manual. Predesigned WT and flange bolt configurations meeting the required geometric and strength criteria are provided in Table 4.

The stiffness of the WT connection between the beam flange and column in the elastic range shall be taken as

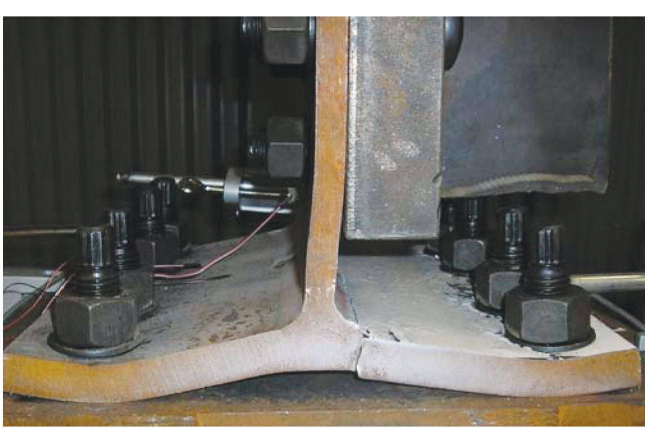

Fig. 13. Example phase 2 flange fracture location.

$$K_e = \frac{142 E p t_{ft}^{\,3}}{3 g^3} \tag{12}$$

where p is taken as 4.5 in. (114 mm).

The stiffness of the WT connection between the beam flange and column in the inelastic range shall be taken as

$$K_p \approx \frac{P_y \left(\omega - 1 \right)}{\Delta_{max}} \tag{13}$$

The expected deformation of the WT at which initial yield occurs, Δ_y, shall be taken as

$$\Delta_y \approx \frac{P_y}{K_e} \tag{14}$$

The load, P, in the WT assembly as a function of deformation, Δ, of the WT assembly to be used to calculate the end rotation of the beam is given as

$$\text{For } \Delta \leq \Delta_y,\ P = K_e \Delta \tag{15}$$

$$\text{For } \Delta > \Delta_y,\ P = P_y + K_p \Delta \tag{16}$$

The stiffness model of the WT assembly is presented in graphical form in Figure 14.

CONCLUSIONS

The following primary conclusions were drawn from the experimental testing.

1. With proper proportioning of WT flange thickness, flange bolt size, WT flange hole size and gage of the flange bolts on the WT, WT moment connections can be detailed in which inelastic deformations are substantially limited to the flange of the WT under large deformations.

2. Improper proportions of the WT flange thickness, flange bolt size, WT flange hole size and gage of the flange bolts on the WT can result in sudden flange bolt failures that could be harmful to the building or its occupants.

3. The geometric criteria presented herein are appropriate to ensure inelastic deformations are substantially isolated to the flange of the WT sections up to an overall target deformation of the WT of 1.75 in. (45 mm).

4. The bi-linear approximation equations recommended herein are appropriate representations of the actual load-deformation characteristics of the WT configurations considered.

Table 4. Predesigned WT and Flange Bolt Configurations					
Section	**Gage on WT, in. (mm)**	**Bolt Diameter, in. (mm)**	**Section**	**Gage on WT, in. (mm)**	**Bolt Diameter, in. (mm)**
WT20×99.5	12 (305)	1.25 (32)	WT7×72.5	11.75 (298)	1.375 (35)
WT18×115.5	12.5 (318)	1.375 (35)	WT7×66	11.25 (286)	1.25 (32)
WT18×67.5	9 (229)	1.125 (29)	WT7×60	10.75 (273)	1.125 (29)
WT16.5×110.5	12.25 (311)	1.375 (35)	WT7×54.5	10.5 (267)	1.125 (29)
WT16.5×100.5	12 (305)	1.375 (35)	WT7×49.5	10 (254)	1 (25)
WT15×86.5	11.5 (292)	1.375 (35)	WT7×45	9.75 (248)	1 (25)
WT13.5×73	10.75 (273)	1.25 (32)	WT6×39.5	9.5 (241)	1 (25)
WT12×52	9.25 (235)	1 (25)	WT6×36	9 (229)	1 (25)
WT7×79.5	12 (305)	1.375 (35)	WT6×32.5	8.5 (216)	0.875 (22)

5. The bi-linear approximation discussed in item 4 is only appropriate for WT configurations meeting the recommended geometric criteria presented.

6. To achieve a joint rotation of 0.04 rad, the maximum nominal beam depth recommended for use with the WT configurations assessed is 30 in. (762 mm), or a W30 wide flange section.

7. The limit states of flange bolt rupture, stem bolt rupture, stem net section rupture, stem block shear rupture and stem compression buckling do not govern the capacity of the WT connection if designed using an AISC LRFD approach to develop the probable strength as determined herein.

8. Experimental testing of beam-column subassemblies using ductile WT connection configurations recommended in Part I should be performed to verify adequate strength and rotational flexibility of bolted-bolted double angle shear connections and to verify the elastic and inelastic rotational stiffness of the connections.

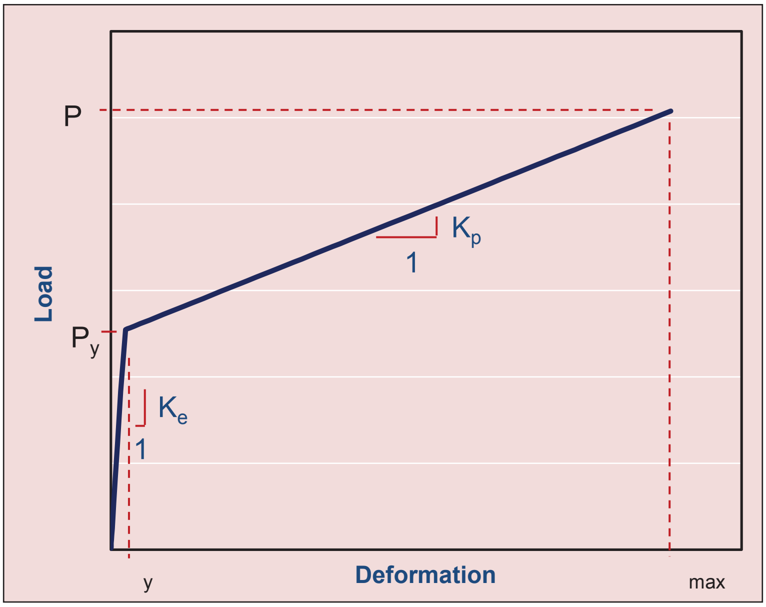

Fig. 14. Bi-linear WT component stiffness.

ACKNOWLEDGMENTS

The authors would like to recognize Puma Steel, AISC, Nucor Fastener and the University of Wyoming for funding, fabrication and material donations, without which this project would not have been possible.

REFERENCES

AISC (2005a), *Seismic Provisions for Structural Steel Buildings*, AISC 341-05, American Institute of Steel Construction, Chicago, IL.

AISC (2005b), *Specification for Structural Steel Buildings*, AISC 360-05, American Institute of Steel Construction, Chicago, IL.

AISC (2005c), *Steel Construction Manual*, 13th ed., American Institute of Steel Construction, Chicago, IL.

AISC (2007), "Double Tee Connections," Draft Provisions Prepared for the AISC Connection Prequalification Review Panel, American Institute of Steel Construction, Chicago, IL.

ASCE 7 (2005), *Minimum Design Loads for Buildings and Other Structures*, ASCE/SEI 7-05, American Society of Civil Engineers, Reston, VA.

FEMA (2000), *State of the Art Report on Connection Performance*, FEMA-355D, Federal Emergency Management Agency, Washington, DC.

FEMA (2003), *Recommended Provisions for Seismic Regulations for New Buildings and Other Structures*, FEMA-450, Part 2: Commentary, Federal Emergency Management Agency, Washington, DC.

FEMA (2008), *HAZUS® MH Estimated Annualized Earthquake Losses for the United States*, FEMA-366, Federal Emergency Management Agency, Washington, DC.

FEMA (2009), *Quantification of Building Seismic Performance Factors*, FEMA-P695, Federal Emergency Management Agency, Washington, DC.

Malhotra, P.K. (2005), "Return Period of Design Ground Motions," *Seismological Research Letters*, SSA, Vol. 76, No. 6, pp. 693–699.

Malley, J.O. (2000), "Future Developments in Seismic Provisions: Life After SAC," Paper prepared for the Fourth International Workshop on Connections in Steel Structures, AISC, Chicago, IL.

McManus, P.M. (2010), "Economic and Serviceable Structural Steel Seismic Load Resisting Systems," in partial fulfillment of the requirement for the Ph.D., Department of Civil and Architectural Engineering, University of Wyoming, Laramie, WY.

Swanson, J.A. and Leon, R.T. (2000), "Bolted Steel Connections: Tests on T-Stub Components," *Journal of Structural Engineering*, ASCE, Vol. 126, pp. 50–56.

Swanson, J.A. and Leon, R.T. (2001), "Stiffness Modeling of Bolted T-Stub Connection Components," *Journal of Structural Engineering*, ASCE, Vol. 127, pp. 498–505.

Swanson, J.A., Kokan, D.S. and Leon, R.T. (2002), "Advanced Finite Element Modeling of Bolted T-Stub Connection Components," *Journal of Constructional Steel Research*, Vol. 58, pp. 1015–1031.